Permeation Process of Small Molecules across Lipid Membranes Studied by Molecular Dynamics Simulations

Siewert J. Marrink* and Herman J. C. Berendsen

Department of Biophysical Chemistry, University of Groningen, Nijenborgh 4, 9747 AG Groningen, The Netherlands

Received: October 5, 1995; In Final Form: July 10, 1996[⊗]

The transport of small molecules across a phospholipid membrane is studied by molecular dynamics simulations. The effects of size, hydrophobicity, and asphericity of the penetrants on the permeation process are investigated. For this purpose, permeability coefficients of oxygen and ammonia are computed using an inhomogeneous solubility−diffusion model and compared to the previously computed results of the permeation of water. Furthermore, solubility and diffusion data are computed for a series of Lennard-Jones particles that differ in size and shape. The results are discussed within the framework of the four-region model and are especially related to the free volume characteristics of the membrane. It is concluded that the free energy of solvation mainly determines the shape of the permeation resistance profile. For hydrophobic particles the membrane interior will act as a trap instead of a barrier. Moderately hydrophilic and hydrophilic penetrants experience the largest resistance to permeation in the dense part of the lipid tail region. This region is therefore most important in discriminating between various penetrants.

Introduction

Recently, we described molecular dynamics (MD) simulations that were performed in order to reveal the permeation process of water across a lipid membrane.[1] It was shown that the permeation process could be modeled with an inhomogeneous solubility−diffusion model, in which both the diffusion rate and the solubility of the water molecule depend on the local position within the membrane. It turned out that the membrane differs significantly from any bulk phase and that the rate-limiting step for the permeation of water is located at the beginning of the lipid tails, the most dense and ordered part of the membrane. Whether a similar permeation process also describes the permeation of other small molecules across the lipid membrane is the topic of this paper.

Experimentally, the range of observed permeabilities for small, nonelectrolyte penetrants is huge: ranging from 10^{1} to 10^{-6} cm/s. The permeability depends on both the solubility of the penetrant into the membrane and the diffusion across. The difference between permeabilities of penetrants can be categorized into three properties: penetrant *size, hydrophobicity*, and *shape*. In order to elucidate the effects of these three properties of the penetrants on both the solubility and diffusion step in the permeation process, we have extended our lipid membrane simulations.[1,2] Part of the computations give detailed, quantitative results, whereas other computations are more oriented toward qualitative insights. The present study is certainly not aiming for a complete analysis of all possible variations of penetrant molecules but is merely trying to give a basic feeling for the way how the nature of the penetrant molecule determines the permeation process.

The importance of *hydrophobicity* is studied by computing the permeability coefficients of oxygen and ammonia, analogous to the method we used for the computation of water permeability. In that way we are able to compare three, almost equally sized, penetrants ranging from completely hydrophilic (water) to completely hydrophobic (oxygen), with ammonia, having a smaller dipole moment than water, in between. The detailed method of simulation will reveal the effects of hydrophobicity on the level of molecular interactions. The effect of *size* on the permeation process is studied by comparing a series of Lennard-Jones (LJ) particles that differ in size. The excess free energy profiles are computed across the entire membrane, the diffusion rates only in the dense region of the lipid tails which is deduced to be the rate-limiting region in the permeation process of most penetrants. Finally, the dependence of membrane permeability on the *shape* of the molecule is studied through comparison of solubility data for a series of connected LJ particles. Because of computational limits, the diffusion rate dependence on penetrant shape was not explicitly studied.

The next section presents a brief review of the experimentally observed trends of penetrant permeation across lipid membranes. Subsequently, the methods of simulation and analysis that are used are described, followed by presentation of the results. Finally, the effects of size, hydrophobicity, and shape of the penetrant on the permeation process are discussed. The discussion takes place within the frame work of the four region model[1,3] and will connect the results to the free volume properties of the simulated lipid membrane (published separately[4]).

Review

In this section we will briefly summarize the experimentally observed and/or theoretically predicted effects of the hydrophobicity, size, and shape of the penetrant molecule on the permeation process across lipid membranes.

Hydrophobicity. The degree of hydrophobicity of a penetrant molecule predominantly affects the solubility part of the permeation process. This is clear from the strong correlation between permeability coefficients and partitioning coefficients in a hydrophobic solvent.[5] The best correlation was originally obtained for bulk hexadecane. Correlation with more polar solvents, like octanol or ether, was found to be not as good. Another, more recent, study[6] shows that correlation with a slightly polarizable solvent as 1,9-decadiene is actually best.

Considering the inhomogeneous nature of the lipid membrane, it is not likely that either the solubility or the diffusion rate

* E-mail: Marrink@Chem.rug.nl.

[⊗] Abstract published in *Advance ACS Abstracts,* September 1, 1996.

S0022-3654(95)02956-X CCC: $12.00

equal a particular hydrophobic solvent throughout the whole membrane. This is supported by the computation of strongly position-dependent solubility profiles for some alkane derivatives.[7] Experimental evidence comes from the observed interfacial resistances that some solutes experience upon permeation[8] and the inhomogeneous equilibrium distribution of nonpolar, alkyl solutes in the membrane.[9] The resemblance between membrane solubility data and solubility data of a particular solvent as hexadecane or 1,9-decadiene can be understood if it applies to a specific membrane region which dominates the resistance to permeation. The large density of hexadecane and the polarizable nature of 1,9-decadiene both point to the densest part of the lipid tail region, i.e., the region behind the headgroups. This region was also identified as rate limiting in the case of our water permeation study.[1]

Size. The effect of penetrant size is difficult to understand even in a qualitative way. Comparing a large series of permeability data, Lieb and Stein[10] showed that for larger penetrants ($50 <$ mol wt < 300) the permeation is not a steep function of size, in contrast to smaller penetrants (mol wt $<$ 50) which show a much stronger size dependence. Walter and Gutknecht,[5] using an even larger data set, showed that the solubility data alone could not explain the size effect on the observed permeation rates. Therefore, they concluded that it should be the diffusion part of the permeation process which accounts for the observed relatively high permeability rates of smaller molecules.

If corrected for the hydrophobicity effect, the observed size dependence of the permeabilities for the larger penetrants is in agreement with the values predicted by the Stokes−Einstein relation for the diffusion rates ($D \sim CV^{-1/3}$ with V the penetrant volume and C a constant that depends on the geometry of the penetrant). For the smallest penetrants, however, the observed size dependence is much steeper, scaling with an exponent of −1.7. Comparing the hydrophobicity-corrected lipid membrane permeability data with diffusion rates across polymers and bulk hydrocarbon, Walter and Gutknecht[5] further concluded that the size dependence of the diffusion process in lipid membranes resembles diffusion in polymers rather than in bulk alkanes.

Experimentally, the slope of the volume dependence of the diffusion process of small penetrants in soft polymers is found to be between −1 and −3 (on a double logarithmic scale), thus incorporating the value of −1.7 found by Walter and Gutknecht in lipid membranes. Similar power law size dependencies are also found by molecular dynamics simulations of soft polymer membranes.[11] Various MD simulations[11−14] show that the mechanism of diffusion of penetrants in polymers is a hopping mechanism. In this mechanism, a penetrant diffuses via jumps between neighboring free volume pockets. Evidence for a hopping mechanism in lipid membranes is found in the recent MD simulations of benzene diffusion in DMPC membranes.[15,16] Jumps of benzene molecules over distances up to 0.8 nm were found, often moderated by torsional changes in the hydrocarbon chains, opening up new free volume pockets for the benzene molecules.

A statistical mechanics study of Xiang and Anderson,[17] however, severely doubts the conclusion that the anomalous size dependence of the lipid membrane permeation process originates in an anomalous (e.g., hopping) diffusion process. They show that the solubility part of the permeation process is also likely to have a size dependency different from that of liquid alkanes. In their subsequent comparative experimental study[6] of permeation rates for a similar set of penetrants as used by Walter and Gutknecht,[5] they conclude that the anomalous steep size dependency of the permeation across lipid membranes can just as well be explained by the solubility step as by the diffusion step. A combination of both mechanisms resulted in an even better quality fit, but this is natural as more adjustable parameters are involved.

Shape. Many penetrant molecules deviate significantly from a spherical geometry, even in the case of the smallest penetrants. For instance, they can be elongated, as in the case of (unbranched) alkanes, or have irregular shapes, as urea. From the regression data of Walter and Gutknecht,[5] no anomalous effect of aspherical penetrants on the solubility part of the permeation process has been noticed, and the same is true for the study of Xiang and Anderson.[6] The observed correlation between membrane and hexadecane or 1,9-decadiene solubility holds also for such elongated molecules as, for instance, hexane derivatives. The statistical mechanical calculations of Xiang and Anderson[17] show a small shape effect predicting that elongated molecules are relatively stabilized in the ordered part of the lipid membrane compared to an isotropic hydrocarbon solvent. However, this shape effect is small compared to the computed size effect of membrane partitioning.

The presence of shape effects on the diffusional part of the permeation process is difficult to extract from the experimental data. For perfectly spherical molecules, the Stokes−Einstein relation (eq 1) predicts a slope of −0.33 for double logarithmic plots of diffusion against volume. Molecules that are nonspherical diffuse slower, as the cross-sectional area and hence the effective friction increase. Now if we assume that larger molecules become more aspherical, this implies a volume dependence of the diffusion constant which is steeper than for purely spherical penetrants. For a series of penetrants that become more globular with increasing volume, the opposite is true. In lipid membranes, Walter and Gutknecht[5] found a slope of −0.88 for a large series of penetrants (excluding the smallest, for which clearly a non-Stokesian behavior is observed), but the quality of the fit was not so good. For the same series a value of −0.5 is predicted by the Stokes−Einstein relation. Assuming that the steep size effect of small molecules is predominantly due to the solubility step, Xiang and Anderson[6] obtain a slope of -0.8 ± 0.3 for diffusion in the membrane compared to -0.74 ± 0.1 in decane. The large error bars prevent any conclusions concerning an anomalous shape effect in membranes compared to liquid alkanes.

Method of Simulation

The simulated membrane is exactly the same as used for the study of the permeation of water[1] and is more elaborately described elsewhere.[2,3] The simulation box contains 64 dipalmitoylphosphatidylcholine (DPPC) molecules in a bilayer configuration, separated by a layer of 736 water molecules (SPC). The boundary conditions are periodic in all three dimensions. The system is coupled to a constant temperature and pressure of 350 K and 1 atm, using weak coupling to an external bath.[18] The membrane force field is all-atom except for methyl and methylene groups that are treated as united atoms. The interaction parameters are based on GROMOS with small modifications.[1,2] The originally obtained lipid charge distribution from ab initio calculations turned out to result in too attractive headgroup−headgroup interactions. Considering the insufficient shielding properties of the SPC water model (especially the high-frequency component), it was therefore decided to divide the lipid charges by a factor of 2. The final simulation conditions are such that the membrane is in the, biologically relevant, liquid-crystalline phase.[2] Recent simulations of DPPC membranes with GROMOS parameters indicate

TABLE 1: Penetrant Parameters σ (nm), ϵ (kJ/mol), q (e), and b_0 (nm)

		σ^e	ϵ^e	q	b_0
H_2O^a	OW	0.317	0.650	−0.820	0.100
	HW	0.000	0.000	+0.410	
NH_3^b	N	0.298	0.877	−0.804	0.1012
	HN	0.000	0.000	+0.268	
O_2^c	O	0.309	0.363	0.000	0.1016
LJ[d]	LJ	0.2−0.6	0.363/0.877	0.000	

[a] SPC model.[21] [b] LJ parameters from GROMOS; bond lengths and charges from quantum mechanical ab initio calculation, reproducing the experimental dipole moment. [c] LJ parameters from Fischer and Lago.[22] [d] LJ parameters based on oxygen or ammonia. [e] Interaction with membrane atoms on basis of standard combination rules: $\sigma_{ij} = (\sigma_i + \sigma_j)/2$ and $\epsilon_{ij} = (\epsilon_i\epsilon_j)^{1/2}$.

that also with full charges a stable liquid-crystalline phase can be obtained, however, using excess water[19,20] (see also Discussion).

In order to compute the permeability coefficients of oxygen and ammonia, four separate runs were performed of 200 ps each. In each of these runs either three oxygens or three ammonia molecules were constrained at fixed positions in the membrane (i.e., six different positions sampled for both oxygen and ammonia). The constraints were applied through resetting of the z coordinates of the particles at every time step to their reference positions. The reference positions equaled the initial positions of the inserted particles except for small fluctuations parallelling the overall scaling of the system due to pressure coupling. The initial z positions of the particles were chosen such as to sample the whole membrane in more or less equidistant steps; the initial xy positions were selected (based on the local free volume distribution[4]) such as to avoid unfavorable overlap with the surrounding atoms.

Part of the final runs were performed on a Cray-YMP, and part on a Convex-240. The additional force field parameters (LJ parameters σ and ϵ and fixed bond length b_0) for oxygen, ammonia, and the LJ penetrants are listed in Table 1, together with the previously used parameters for the water penetrant.

The method of computation of the permeability coefficients of oxygen and ammonia is the same as described in the previous study for the permeation of water.[1] In order to compute the permeability coefficients, we used an inhomogeneous solubility−diffusion model in which both the excess free energy ΔG and the diffusion rate D of the penetrant depend on the position z within the membrane:

$$1/P = \int_{z_1}^{z_2} R(z)\,\mathrm{d}z = \int_{z_1}^{z_2} \frac{\exp(\Delta G(z)/kT)}{D(z)}\,\mathrm{d}z \qquad (1)$$

Here $R(z)$ denotes the local resistance of the membrane, and P is the experimentally accessible permeability coefficient. The theoretical derivation of the inhomogeneous solubility−diffusion model[1] is valid for other small penetrants as well, as long as the thermodynamic gradients remain small.

In order to compute the local excess free energy $\Delta G(z)$, we applied both the method of particle insertion (PI) and the method of constrained particles (CP). The method of particle insertion samples the relevant phase space through random insertions of the penetrant molecule in the membrane. From the difference between the insertion chemical potential in the membrane and in the bulk $(z = 0)$ the excess free energy can be obtained through

$$\Delta G^{\mathrm{PI}}(z) = \Delta\mu^{\mathrm{ins}}(z) - \Delta\mu^{\mathrm{ins}}(0) \qquad (2)$$

where

$$\Delta\mu^{\mathrm{ins}}(z) = -kT \ln \langle \exp(-E^{\mathrm{ins}}(z)/kT)\rangle \qquad (3)$$

is the average Boltzmann factor of the random inserted test particle. (E^{ins} denotes its interaction energy.) The method gives qualitatively correct results in the less dense parts of the membrane only but can provide qualitative insights in the denser regions, too. The statistics of the method can be increased by using a free volume based biasing procedure.

The method of constrained particles can be applied to obtain quantitative good results in the dense parts of the membrane also but is computationally more costly. A potential of mean force can be contructed by constraining the penetrant particles in different regions of the membrane, measuring the average force $\langle F_z(z)\rangle$ (in the direction of the constraint) needed to keep the constraint, and integrate across the membrane:

$$\Delta G^{\mathrm{CP}}(z) = \int_0^z \langle F_z(z)\rangle\,\mathrm{d}z \qquad (4)$$

As free energy differences can be added, both methods can be easily combined. Assuming that the constrained particle method is applied from $z = 0$ to $z = z_1$ and the particle insertion method from $z = z_1$ to z, combination of the above equations yields

$$\Delta G(z) = \Delta G^{\mathrm{CP}}(z_1) + \Delta G^{\mathrm{PI}}(z) - \Delta G^{\mathrm{PI}}(z_1) = \int_0^{z_1} \langle F_z(z')\rangle\,\mathrm{d}z' + \Delta\mu^{\mathrm{ins}}(z) - \Delta\mu^{\mathrm{ins}}(z_1) \qquad (5)$$

The choice of z_1 can be determined by comparing the magnitude of the statistical errors of both methods. The PI method will normally provide smallest errors in the less dense regions whereas the CP method is expected to be most accurate in the dense regions. Note that a third method that could be used in the case of water permeation, based on analysis of local equilibrium densities, is of no value in the case of other penetrants.

Diffusion constants can be normally computed in MD simulations most easily from the slope of the mean square displacement curve. However, this method fails to work if thermodynamic gradients are present. In such cases the force correlation method can be applied to compute the local diffusion constants. This method relates the time fluctuations of the instantaneous force $\Delta F_z(z,t)$ on a constrained particle (in the direction of the constraint) to the local time-dependent friction coefficient $\xi(z,t)$, from which the local diffusion constant in the z direction $D_z(z)$ can be obtained by time integration:

$$D_z(z) = RT/\int_0^\infty \xi(z,t)\,\mathrm{d}t = (RT)^2/\int_0^\infty \langle \Delta F_z(z,t)\,\Delta F_z(z,0)\rangle\,\mathrm{d}t \qquad (6)$$

A concomitant advantage of this method is that it also constraints a penetrant molecule in the membrane, similar to the contrained particle method. Therefore, the local diffusion constant and the derivative of the free energy profile can be computed simultaneously. For more details of the applied methods we refer to the water permeation study.[1]

Due to the symmetry of the membrane, the locally computed properties in one half of the membrane are valid for the other half of the membrane as well. For reasons of clarity, the presented figures show profiles across the whole membrane that are symmetrized around the middle. Error bars represent statistical errors (see Discussion).

Results

In this section the results of the various computations are presented. In order to facilitate the discussion, the results are

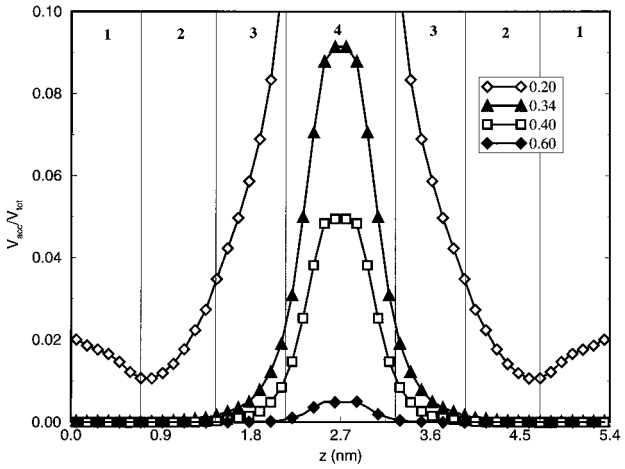

Figure 1. Accessible free volume distribution across the membrane of spherical penetrants with diameters ranging from 0.2 to 0.6 nm. The middle of the water layer is located in region 1.

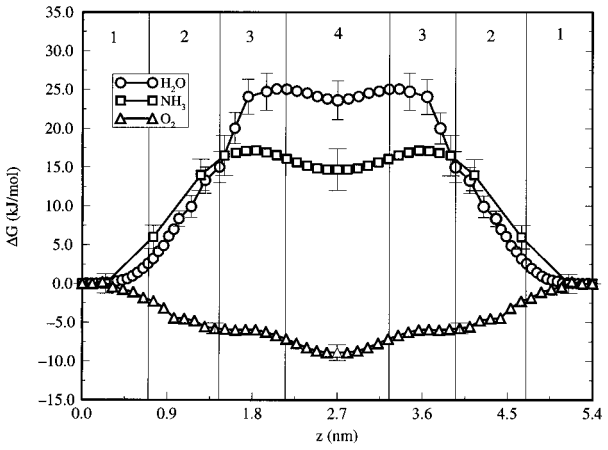

Figure 2. Excess free energy profiles of water, ammonia, and oxygen. The middle of the water layer is located in region 1.

presented within the framework of the four-region model. This is a qualitative model, based on our simulation results of the lipid membrane in combination with relevant experimental and theoretical data, that divides the membrane into four distinct regions. Region 1 is the region in which the membrane headgroup density is still low and is characterized mainly by loosely bound water molecules attached to choline headgroups. In region 2 the headgroup density is high, and the water molecules present in this region are strongly bound. It also contains the major part of the glycerol backbones. Region 3 contains the more ordered part of the lipid tails, with a density larger than liquid hexadecane. Region 4, finally, contains the major part of the lipid end groups. This region is much more disordered and therefore has a low density. Regions 1 and 2 are also referred to as the interface of the membrane, and regions 3 and 4 as the membrane interior. More details about the four-region model, including graphical representations, can be found in the previous publications.[1,3]

We will also make an extensive use of our analysis of free volume properties in the lipid membrane.[4] Many observed effects can be related to these free volume properties. In terms of free volume properties, both interfacial regions 1 and 2 are similar and can be characterized as isotropic, containing many small, spherical holes. Region 3 resembles a soft polymer, due to a strong correlation between the lipid chains that is imposed by the lipid headgroups. Therefore, larger free volume pockets are relatively stabilized (although the total free volume remains small). The free volume is distributed anisotropically, with an enhanced probability of finding a free volume pocket extended along the membrane normal. Largest free volume pockets are found in region 4. In contrast to region 3, these are isotropically oriented. In Figure 1 we have displayed the accessible free volume, V_{acc}, as a fraction of the total volume, V_{tot}, for a number of spherical penetrants in different regions of the membrane. Details about the free volume properties can be found in the original publication.[4]

Water, Oxygen, and Ammonia. In order to reveal the effect of hydrophobicity on the permeation process, we computed the excess free energy profiles and diffusion rate profiles of ammonia and oxygen. The results obtained for water in a previous study[1] are added for comparison.

The excess free energy profiles of water, ammonia, and oxygen in the lipid membrane are shown in Figure 2. The profile for ammonia is calculated from the constrained particle method in regions 1 and 2 and from the particle insertion method in regions 3 and 4. For the oxygen profile the insertion method yielded most accurate results in all regions, due to the absence of electrostatic interactions.

If we compare the excess free energy profiles of water and ammonia, it turns out that the shapes of both curves are very similar. The main difference is the total height of the barrier, which is ≈10 kJ/mol lower in the case of ammonia. This difference originates from the fact that the dipole moment of ammonia is much smaller than that of water (in our force field $\mu_{H_2O} = 2.27$ D vs $\mu_{NH_3} = 1.47$ D). From the experimental value[23] of the partition coefficient of ammonia between water and bulk hexadecane, we calculate a solvation free energy of 15 kJ/mol at $T = 300$ K. This value is similar to the values we calculate in the membrane interior. Just as in the water profile, the ammonia profile also shows a pronounced dip in region 4, which we contribute to the lower local density or larger accessible free volume (Figure 1). Another interesting observation is the fact that both the water and ammonia profiles increase with about the same slope in regions 1 and 2, whereas in region 3 the water excess free energy continues to increase, unlike the excess free energy of ammonia. If the magnitude of the dipole moment would be the sole factor determining the local excess free energy, one would have expected the slope of the water profile to be larger in regions 1 and 2 also. In our view, a plausible explanation would be that the water molecules are able to form stronger hydrogen bonds with the headgroup atoms and/or with the other water molecules, resulting in a relatively lower excess free energy in regions 1 and 2.

The excess free energy profile of oxygen is completely different. Being a hydrophobic penetrant, i.e., lacking electrostatic interactions, the oxygen molecule prefers to dissolve into the membrane interior. The shape of the excess free energy profile is complementary to the accessible free volume profile of the membrane (Figure 1) and similar to the free energy profile of water in the absence of electrostatic interactions.[1] The value of the excess free energy of oxygen in the middle of the membrane is close to the excess free energy of oxygen in the gas phase relative to aqueous solution, −10.7 kJ/mol at $T =$ 323 K, computed from the partition coefficient of oxygen between the gas phase and water.[23] An average value for the excess free energy of oxygen in the membrane can be computed from the partition coefficient of oxygen between water and lipid membrane,[24] which results in −3.7 kJ/mol at $T = 300$ K. The value that we obtain, averaged over the whole membrane (from $z = 0.0$ to $z = 5.4$), is −4.5 kJ/mol, which is close to the experimental result. Note, however, that the definition of membrane boundaries, as well as the temperature difference between the experimental and MD data, makes a fair comparison difficult.

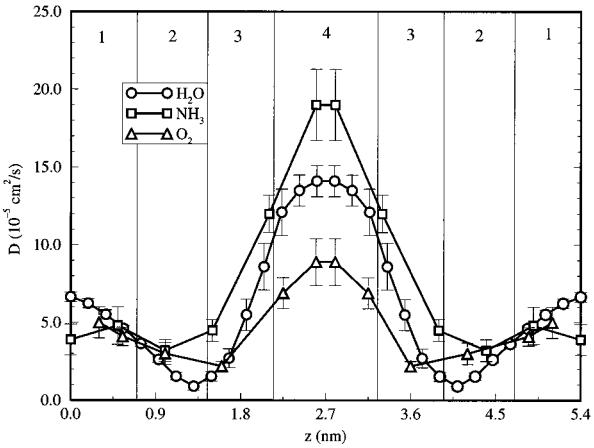

Figure 3. Diffusion rate profiles of water, ammonia, and oxygen. The middle of the water layer is located in region 1.

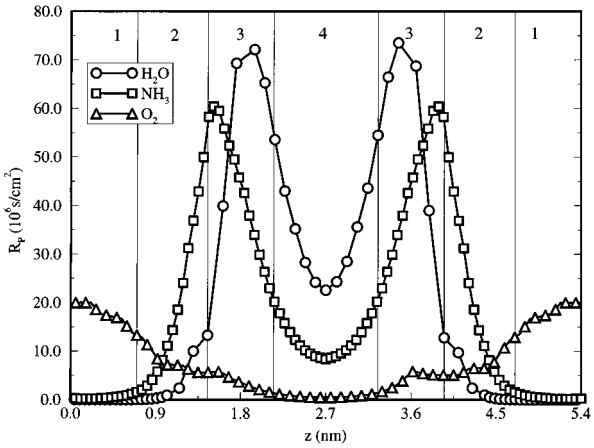

Figure 4. Local resistance to permeation of water, ammonia, and oxygen in the membrane. The middle of the water layer is located in region 1. For reasons of clarity, the profiles of ammonia and oxygen are scaled by a factor of 10 and 10^4, respectively. To match the diffusion data with the free energy data and to improve integration of the resistance profiles, additional points have been interpolated.

The results of the diffusion rate calculations of ammonia and oxygen, using eq 6 at various positions in the membrane, are shown in Figure 3. The previously computed diffusion rate profile of water[1] is also included. As can be clearly seen from this figure, the diffusion pattern for all three penetrants is similar. Highest diffusion rates are found in region 4, where the membrane density is lowest, and much lower diffusion rates in region 2, the region of large headgroup density. The minima in the profiles are not completely located at the same position. However, considering the error bars, the observation of an inward shifted minimum for oxygen diffusion is not significant. In the membrane interior, the diffusion of ammonia is observed to be highest and that of oxygen to be lowest. This clearly points to a size effect, ammonia being the smallest penetrant and oxygen the largest.

Experimentally, the direct measurement of diffusion rates of small penetrants within the membrane is not possible. From fluorescence measurements,[25] however, a value of $D = 1.54 \times 10^{-5}$ cm^2/s was derived for oxygen diffusion in DPPC membranes in the liquid crystalline phase (at $T = 318$ K). Temperature-dependent measurements of the same authors revealed a surprisingly small, activation energy of ∼4.4 kJ/mol for oxygen diffusion in a liquid crystalline DPPC membrane. Assuming an Arrhenius type of temperature dependence, we estimate a value of $D \approx 2 \times 10^{-5}$ cm^2/s at $T = 350$ K. This value is somewhat smaller than the average value that we find, which is 4.7×10^{-5} cm^2/s. Considering the experimental uncertainties and the uncertainties in the force fields that we used, the agreement is good.

We can also compare the diffusion rates of oxygen in the membrane interior to the diffusion rates of oxygen in bulk alkanes. In cyclohexane,[23] a value of 5.3×10^{-5} cm^2/s is reported at $T = 300$ K. Using the same temperature correction as described above, a value of $D \approx 7.5 \times 10^{-5}$ cm^2/s results at $T = 350$ K. Considering the density of cyclohexane, this value should be similar to the value we find in region 4, where the density is comparable. On average, $D = 8 \times 10^{-5}$ cm^2/s in region 4, so in this case the agreement is even better.

The results for oxygen diffusion may also be compared to the simulation of oxygen diffusion through a monolayer of constrained hexadecane molecules, modeling a lipid membrane.[26] In this study, it was shown that the resistance to diffusion in the constrained part of the system (modeling the headgroup region) was considerably larger than in the free part, in qualitative agreement with our profile. The mean value for the oxygen diffusion coefficient in the hexadecane system was computed to be $D = 2.6 \times 10^{-5}$ cm^2/s at $T = 300$ K. Applying the temperature correction, the value at $T = 350$ K is extrapolated to be 3.7×10^{-5} cm^2/s, close to our averaged value of 4.7×10^{-5} cm^2/s. Unfortunately, we did not find any experimental data on ammonia diffusion, neither in membranes nor in bulk alkanes.

Although the diffusion profiles for ammonia, oxygen, and water are very much the same, this does not automatically imply that also the time-dependent friction coefficients are similar. Different diffusional mechanisms could in principle result in the same diffusion coefficients. Comparison of the local time-dependent friction coefficients for ammonia and oxygen, with those of water,[1] revealed that the diffusional mechanism is similar for these penetrants. In regions 1 and 2 the frictional forces are high. Fitting the curves to exponentials resulted in decay times that are short (∼0.1 ps). In region 3 also high frictional forces are observed, but the curves had to be fitted to two exponentials, characterized by a very short decay time (<0.1 ps) and a longer one of ∼2 ps. This double exponential decay in region 3 is also observed for the LJ particles (of different sizes, see Figure 6), and may result from the constrained motion of the penetrants in their local free volume pockets. In region 4, the frictional forces are much smaller, and only one exponential is needed to fit the curves. The resulting decay times in region 4 are on the order of 0.5 ps. As we discussed in our water permeation study,[1] the small values of the correlation times imply that the motion of the penetrants across the membrane is diffusive for these kind of molecules; inertia effects can be neglected.

From the local diffusion rates and the local excess free energy, we can now compute the local resistance to permeation according to eq 1. In Figure 4, the local resistances that are experienced during the membrane permeation process of water, ammonia, and oxygen are shown. As we already noticed in the case of water permeation, the shape of the resistance profiles are mainly dominated by the shape of the excess free energy profiles. Only the dips in the middle of the membrane are clearly enhanced due to the fast diffusion rate in this region. The permeation resistance is largest in the case of water permeation, as a result of the low equilibrium concentration of water in the membrane. Both ammonia and water have a maximum of the permeation resistance in region 3, which is shifted somewhat inward for water with respect to ammonia. The origin of this shift can be found in the excess free energy profiles, where we observed the same shift of the maxima and

which we attributed to the weaker hydrogen bonding capacities of ammonia with respect to water.

In the case of oxygen, the maximum resistance to permeation is not located in the membrane, but in the water layer. For such a hydrophobic penetrant, the concentration in the membrane is larger than in the more hydrophilic regions, and the membrane behaves as a permeation "accelerator" instead of a permeation barrier.

Integration of the resistance profiles over the membrane results in the total permeation resistance, which is inversely related to the permeability coefficient (eq 1). For ammonia we compute a value of $P_{NH_3} = (9 \pm 6) \times 10^{-1}$ cm/s, which is 1 order of magnitude larger than the permeability coefficient of water, which was found to be $P_{H_2O} = (7 \pm 3) \times 10^{-2}$ cm/s. In the literature we only found measurements of the permeability coefficient for ammonia through egg-PC. A value of $P_{NH_3} = (1.3 \pm 0.4) \times 10^{-1}$ cm/s is reported using an electrical method which is based upon the fact that net fluxes of weak acids or weak bases produce pH gradients in the unstirred layers adjacent to the membrane, which can be measured with a suitable protonophore.[5] A smaller value of $P_{NH_3} = 3.7 \times 10^{-2}$ cm/s, using the same method, has also been reported.[27] Since both measurements were performed at room temperature, we need a temperature correction in order to compare our value with the experimental ones. Since there are no activation energies reported for the permeation process of ammonia, we base our estimate on the activation energy we used to compare the water permeability with the experimental data, which was 45 kJ/mol.[1] Assuming that the activation energies of the diffusion process are similar for water and ammonia, and using the calculated difference of ~10 kJ/mol for the excess free energies of both penetrants, we estimate the activation energy for ammonia to be 35 kJ/mol. From an Arrhenius type of temperature dependence, the experimental data are then converted to $P_{NH_3} = 9 \times 10^{-1}$ cm/s[5] and $P_{NH_3} = 3 \times 10^{-1}$ cm/s[27] at $T = 350$ K. Although the temperature correction factor remains quite uncertain, and the permeabilities are measured across egg-PC instead of pure DPPC, the value that we calculate seems to be on the right order of magnitude.

For oxygen, we calculate a permeability coefficient of $P_{O_2} = (2 \pm 5) \times 10^2$ cm/s across the the whole membrane (from $z = 0.0$ to $z = 5.4$). This value is clearly much faster than for the more hydrophilic penetrants. Note that the calculated value depends very much on the position of the integration boundaries. Whereas in the case of ammonia and water permeation the resistance in the water layer is practically zero, this is not the case for oxygen. If we integrate only over regions 3 and 4, the permeability coefficient becomes even larger: $P_{O_2} = (15 \pm 4) \times 10^2$ cm/s.

To our knowledge, no experimental permeability measurements are performed in the case of oxygen. This is not surprising as the permeation resistance for oxygen in the membrane is negligible compared to its resistance in water. Therefore, standard permeability measurements are impossible. However, we can estimate a permeability coefficient from fluorescence measurements in artificial DPPC membranes.[25] In these measurements, the decay of pyrene fluorescence due to quenching by oxygen was measured, which can be related to the product of oxygen diffusion rate and oxygen concentration in the membrane. The permeability coefficient can be obtained by dividing this number by the width of the pyrene-probed region of the membrane. A difficulty is that it is not completely clear which parts of the membrane are probed by the pyrene molecule. Assuming that the concentration of pyrene is homogeneous across regions 3 and 4 and negligible in regions 1 and 2, we estimate a permeability coefficient of $P_{O_2} = 2.7 \times 10^2$ cm/s at $T = 298$ K. This value has to be compared with the value of $P_{O_2} = (15 \pm 4) \times 10^2$ cm/s that we computed across regions 3 and 4. The temperature correction will be small in this case, as the activation energy for oxygen diffusion is measured in the same study to be only 4.4 kJ/mol, which is largely canceled by the average excess free energy of oxygen in the membrane. The difference of roughly a factor of 5 between our data and the data derived from the experiment therefore has to be attributed to the uncertainties in the experimental as well as in the computational methods.

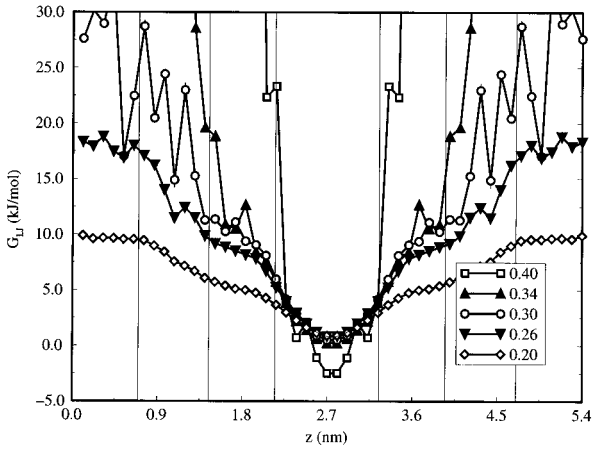

Figure 5. Free energy profiles of a series of LJ particles with different sizes, based on oxygen. The middle of the water layer is located in region 1.

Series of LJ Particles. The excess free energy profiles (with respect to an ideal gas phase) of a series of LJ particles with different sizes give information about the size dependency of the solubility process. These LJ profiles, which are computed with the particle insertion method, are plotted in Figure 5. The LJ interaction parameter ϵ is based on the one that we used for oxygen. The parameter σ is increased from 0.2 to 0.6 nm. Note that the values obtained in the dense parts of the membrane are subject to systematic errors, especially for the larger penetrants. (Therefore, the profiles for LJ particles with $\sigma > 0.4$ nm are not shown.) Real free energies in those regions will be lower. The qualitative features are presumed to be realistic, however.

Comparing the LJ particles with different sizes, one sees that the larger penetrants are relatively stabilized in region 4, the center of the bilayer. This is clearly a result of the large amount of accessible free volume in this region (Figure 1). Even penetrants with diameters larger than 0.5 nm (not shown) seem to fit into free volume holes large enough to allow for a favorable excess free energy in this region. The high-density lipid region 3 shows a much steeper size dependence, similar to that of regions 1 and 2.

To study the effect of asphericity on the solubility step, the free energy profiles for a series of connected strands of LJ particles (based on atomic oxygen, see Table 1) were computed. Note that the strands were taken to be rigid; i.e., no sampling of internal conformations was allowed. Again the particle insertion method was used, implying quantitatively accurate data inside the membrane only. The results for strands of one (atomic oxygen), two (molecular oxygen), three, and five LJ particles are compared in Figure 6.

The aspherical particles show a different trend in comparison with the trend seen in the previous figure. If the size of the penetrant is increased in an aspherical way (i.e., connecting LJ particles as a strand), region 3 stabilizes relatively more than

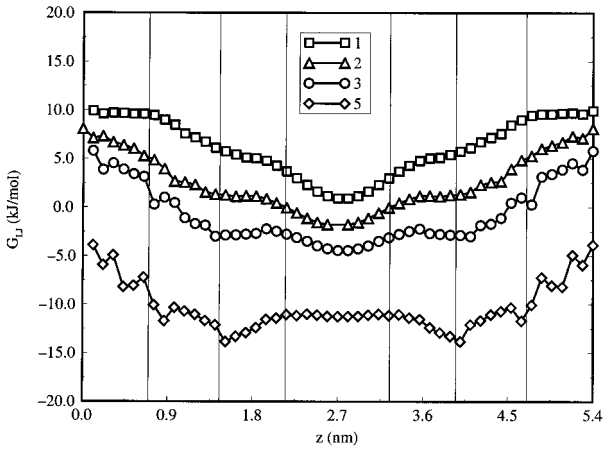

Figure 6. Free energy profiles of rigidly connected linear strands of 1, 2, 3, and 5 LJ particles, all based on oxygen. The middle of the water layer is located in region 1.

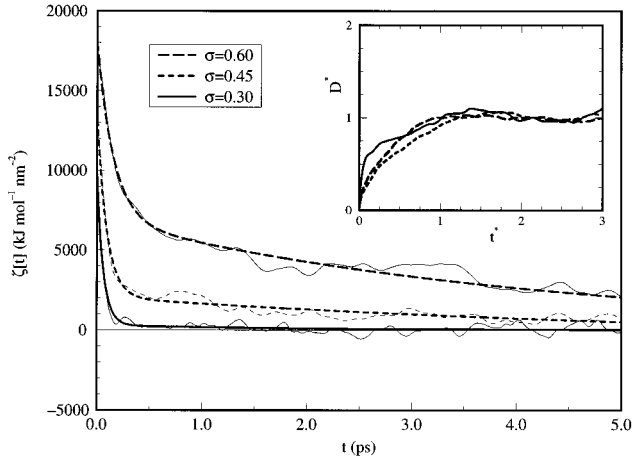

Figure 7. Time-dependent friction coefficients in region 3 for LJ particles with different sizes. Smooth lines are fits to double-exponential functions. The inserted graph shows the convergence of the relative diffusion constant $D^* = D(t)/D(\infty)$ against relative time $t^* = t/t^{long}$.

region 4. In the case of "pentaoxygen", region 3 is even preferred above region 4 considering the excess free energies.

The effect of penetrant size on the diffusion rates in the membrane is studied through the comparison of three LJ particles (based on the moderately hydrophilic penetrant ammonia, see Table 1) that differ in size. The penetrant diameters were taken as 0.3, 0.45, and 0.6 nm. Due to computational limitations, the diffusion rates were only evaluated in region 3 of the membrane. Since the rate-limiting step is located in this region for most penetrant molecules (see Discussion), the size dependence of the diffusion rate in region 3 is most important for understanding the general permeation process. The method that was used is the force correlation method. For every penetrant size a simulation of 120 ps was performed, with three penetrants constrained in region 3 of the membrane. The time-dependent friction coefficients, averaged over the three penetrants, are shown in Figure 7. The figure shows that the friction in region 3 increases upon increasing penetrant size. The static friction coefficient is proportional to the area underneath the time-dependent friction coefficient. Both the height of the frictional forces and the longer decay time contribute to the larger friction experienced by larger penetrants. All curves could be fitted to double exponentials, one with a short decay time ($t^{short} = 0.1-0.2$ ps in all cases) and a long decay time t^{long} of 2 ± 0.5, 6 ± 1, and 10 ± 2 ps for the smallest, medium, and largest penetrant, respectively. The short decay time arises from the immediate response to the local environment of the particles, i.e., the friction due to the surrounding lipids that keep the particles in their local cage. The interpretation of the long decay times is not so straightforward, however. Considering the resemblance between region 3 of the lipid membrane with a soft polymer,[4] one would expect a hopping type of diffusion, and the long decay times can be interpreted as average residence times of the penetrants in their free volume pockets. Our results then indicate that the time between subsequent hops increases with penetrant size, in agreement with the intuitive picture. Small penetrants will make many small jumps, and large penetrants will make few, larger jumps.

The increased friction for larger penetrants results obviously in lower diffusion rates. The insert in Figure 7 shows the time evaluation of the integral in eq 6, showing the convergence of the computed diffusion coefficient for times longer than the largest correlation time. We derived values of $D_z = (8 \pm 1) \times 10^{-5}$, $(10 \pm 2) \times 10^{-6}$, and $(3 \pm 0.5) \times 10^{-6}$ cm^2/s for the small, medium, and large penetrant, respectively. Comparing these results with the experimental trend of a steep size dependence for the smallest particles (up to ~0.5 nm) and a less steep size dependence for the larger ones, we can conclude that our results reproduce this trend in region 3 of the membrane. It should be noted that the force correlation method becomes more unreliable as the size of the penetrants increases. In the case of the largest penetrant we observe a substantial correlation time (on the order of 10 ps), and the limit of overdamped Markovian dynamics may be in reach. In that case inertia effects become important for an accurate description of barrier crossing rates.

Discussion

Errors. Inevitably connected to the method of MD simulations is that the results are sensitive to force field parameters and simulation time. Wrong parameter choices or insufficient sampling may lead to systematic errors. In utopia one could eliminate such errors by sampling a few microseconds and comparing a dozen different force fields, but this is not a realistic approach nowadays. However, the following arguments should indicate that our force field and simulation time are sufficient to validate our conclusions.

Mean field MD simulations[28] of lipid membranes have indicated that correlation times of more than 1 ns exist (e.g., lipid wobbling motions), which are certainly not adequately sampled in the trajectory that we used for our present computations. It is therefore necessary to make an estimation of the importance of these long time lipid modes on the properties of the membrane. During a series of simulations of DPPC membranes with similar force field parameters as we used in the present study, we have already reached a total simulation time of several nanoseconds. During these simulations we have tested a number of membrane properties upon the appearance of significant changes. All of the calculated properties, including lipid headgroup area, atomic distributions, and free volume distributions, remained rather close to those of the original simulation. Therefore, we conclude that the trajectories analyzed in this paper have a distribution of membrane conformations representative of the equilibrium state. Long time correlations seem to be not very important for the main characteristics of any of the membrane regions. The penetrant properties that we have calculated, such as diffusion rates and excess free energies, also showed a reasonably good convergence in most cases (except for the results in Figures 5 and 6, which only have qualitative value). Apparently, the dominant penetrant−membrane interactions are determined by short time relaxation processes, such as position correlation times of water (in regions 1 and 2) or transitions of dihedral angles (in regions

3 and 4). Therefore, the presented errors are statistical errors obtained from a division of the trajectory into separate intervals corresponding to these relaxation times. From our water permeation study,[1] we have deduced that in region 1 the water is on average only weakly bound to headgroup atoms, resulting in a correlation time of ∼5 ps. In region 2 the hydration is stronger, with correlation times of 30 ps on average. Analysis of dihedral transition times[2] revealed lifetimes of ∼30 and ∼10 ps for regions 3 and 4, respectively. Thus, in order to determine the statistical errors, the trajectory was divided into subtrajectories of 5, 30, 30, and 10 ps for regions 1−4, respectively.

On first sight it might seem surprising that convergence times for penetrant diffusion in polymers often requires simulation times of several nanoseconds.[11,29] There is, however, an important difference. These long convergence times in polymer simulations originate from the long-range correlations in the polymer matrix, which initially result in fractal diffusive behavior. Only after long sampling times has the penetrant lost its memory of the initial fractal environment, and normal diffusion is observed. In lipid membranes, however, such long-range correlations are not present. Considering diffusion in the perpendicular direction only, the part of the membrane which resembles a polymer measures less than 1.0 nm width. Therefore, fractal diffusion as is observed in polymers is not important in lipid membranes, and convergence can be achieved much more rapidly.

Regarding the choice of force field, recently the equilibrium properties of a number of DPPC membrane systems with both SPC and SPC/E water model and with full and reduced charges have been compared.[20] It was concluded that the SPC−membrane interface is somewhat broader than the SPC/E−membrane interface, which can be attributed to the difference in chemical potential of both water models. Since the chemical potential of SPC is closest to the experimental value for bulk water, the SPC model is to be preferred for free energy calculations. On the other hand, the SPC/E model describes the diffusional behavior of water better. In the DPPC simulations, a difference of roughly a factor of 1.5 between the diffusion constants of SPC vs SPC/E was found across the whole interface. As the permeation resistance is determined mainly by the free energy profile, we conclude that the resistance to permeation for SPC/E would be somewhat larger than for SPC. The comparison of full headgroup charges with reduced charges led to the conclusion that actually full charges can produce a stable liquid-crystalline phase, using furthermore the same parameters as we do except for the presence of an excess water layer. The resulting interfacial atom distributions are, however, similar to ours. The width of the interface, for instance, defined as the distance over which the water density drops from 90% to 10% of its bulk value, is 1.3 nm in our simulation and 1.2 nm in the full charge simulation. Also, the electron density profile and the lipid order parameters are similar to ours (and also similar to results of MD simulations of closely related membranes). Although we do not fully understand the effects of the magnitude of the lipid charges and the amount of water—probably a rather delicate electrostatical balance between headgroup−headgroup interactions in the same and in opposite halves of the bilayer exists—we believe that a different force field would not significantly change the results. We note again that most of the results should be interpreted primarily in a qualitative way.

In the folowing sections we will systematically discuss some characteristics of the dependence of the permeability process on the hydrophobicity, size, and shape of the penetrant molecule as it follows from the presented simulation results.

Hydrophobicity. The large hydrophobicity dependence of the permeation process is reflected very clearly in the differences in permeation resistance for water, ammonia, and oxygen (Figure 4). Especially the difference between a completely hydrophobic penetrant on one hand (oxygen) and the more hydrophilic penetrants on the other (ammonia and water) is large. Whereas for the hydrophilic penetrants the rate-limiting step for permeation is located in region 3, the dense part of the lipid tails, the rate-limiting step for the hydrophobic penetrant is the passage of the water layer, and not the membrane itself. The origin of this difference is almost entirely due to the differences in membrane solubility. The excess free energy profiles (Figure 2) show that the average solubilities of the penetrants in the membrane interior, i.e., regions 3 and 4, are close to the excess free energies of solvation into hexadecane. This is in agreement with the experimentally observed strong correlation between penetrant permeation rates and partition coefficients between hexadecane and water.[5,10] The even better correlation with the slightly more polar 1,9-decadiene[6] was reason to believe that the rate-limiting step of the permeation process of the experimentally studied penetrants (i.e., penetrants that are at least moderately polar) lies in region 3, which is more polar due to the adjacent membrane/water interface. Our results for water and ammonia underline this picture.

Size. The excess free energy profiles, computed for a series of LJ particles, reaffirm the fact that the membrane interior differs considerably from a homogeneous alkane phase. Especially in the middle of the membrane, the solubility remains high for larger penetrants, due to the large fraction of accessible free volume in region 4 (see Figure 1). As a consequence, we expect the location of the rate-limiting step in region 3, the high-density part of the lipid tails, even more pronounced for larger (hydrophilic) penetrants than for smaller ones.

According to Xiang and Anderson,[6] part of the anomalous (i.e., steep) size dependency of membrane permeation originates possibly from the dissolvation into region 3. Experimentally, Walter and Gutknecht[5] observed a strong resemblance between the size dependency of the permeation across lipid and polymer membranes. In our free volume study[4] we have showed that the free volume properties in region 3 of the membrane are indeed close to those of a soft polymer. Not only are the density and total free volume similar, but also the accessible hole size distribution and the scaling behavior of the accessible free volume. Therefore, one can expect that the local environment for a penetrant in the soft polymer is very similar to that of region 3 of the membrane. The size distribution of the free volume pockets in this region obeys an extended power law decay, indicating a relatively large amount of free volume accessible to small penetrant molecules. This would facilitate the solvation step for the smallest penetrants considerably compared to their solubility into a bulk hydrocarbon solvent. Unfortunately, our solubility data in region 3 are not accurate enough to extract a quantitative relationship between solubility and size.

The anomalous size dependency could also originate (partly) from the diffusional part of the permeation process. Our computation of diffusion rates in region 3 of the membrane indicates a rather steep size dependency, steeper than predicted by the Stokes−Einstein relation. The double-exponential decay of the time-dependent friction coefficients (Figure 7) probably points to a hopping type of diffusion in region 3. The longer decay time can be interpreted as the typical time that the penetrants are captured in a specific free volume pocket for a while, which is a prerequisite for hop diffusion. The observed increase in this correlation time with penetrant size (from 2 to

10 ps for penetrants with diameters from 0.3 to 0.6 nm) agrees with the intuitive picture of less frequent hops for larger molecules. In polymers, direct evidence for hop diffusion arises from various simulation studies.[11−14] The reason for hop diffusion in polymer membranes is the presence of very slow rearrangment times of the polymer matrix, in combination with relatively long-range order. The available free volume is therefore rather static, and a penetrant molecule diffuses fastest by making jumps from one free volume pocket to the next. On the contrary, in bulk liquid hydrocarbons, the reorientation times of the hydrocarbon chains (and thus the free volume!) are much faster. In this case, a normal diffusion process can take place in which small displacement steps are made continuously. In region 3 of the lipid membrane, resembling a soft polymer, also large reorientation times exist. This can be concluded from the less frequent trans−gauche transitions in this region.[2] Relatively slow relaxation times of lipid order at the beginning of the lipid tails have also been concluded from MD simulations of a DPPC bilayer compared to bulk hexadecane.[30] Therefore, hop diffusion is likely to be the dominant type of diffusion in the dense and ordered parts of the lipid membrane as well. MD simulations of benzene diffusion in a DPPC membrane[15,16] clearly show the occurrence of occasional jumps. Note that for larger penetrants, which locally distort the lipid environment, i.e., penetrants that are larger than the local correlation length of the lipid matrix, a normal nonhopping diffusion process (following Stokes−Einstein relation) may begin to dominate.

Shape. The largest anisotropy of the membrane is found in region 3, and also the free volume in this region shows anisotropic behavior.[4] As a result, the main difference between the permeation process of nonspherical particles vs spherical particles will originate from region 3. Since this is also the region which dominates the permeation process itself for most of the experimentally accessible penetrants, one could expect that even small differences in molecular geometry are reflected in the permeation process. The effect of an elongated shape of the penetrant on the excess free energy profile is illustrated in Figure 6, where we showed that the elongated shape results in a relative stabilization in region 3. (Although we only used hydrophobic penetrants to study this effect, we assume that this will also be the case for hydrophilic penetrants.) This stabilization is a direct result of the possibility for an elongated penetrant to have more favorable LJ interactions when it resides in an aspherical free volume pocket. This may also account for the experimentally observed feature that flat molecules have a relatively more favorable enthalpic interaction with the membrane interior than with a bulk alkane solvent.[31,32] This observation has led to the concept of a "nonclassical" hydrophobic effect, indicating that enthalpy is the driving factor for nonpolar solute partitioning into lipid membranes, instead of entropy as in the case of the normal, "classical" hydrophobic effect. From our data, we conclude that it is especially region 3 from which the nonclassical effect originates.

We did not study the effect of penetrant shape on the diffusion process directly. On the basis of the free volume study,[4] which showed that in region 3 the free volume pockets are more elongated with their long axis oriented along the *z* direction, we expect that more elongated penetrants will have an accessible free volume which is higher. Therefore, the diffusion rates are expected to be larger than predicted from their effective diameter, i.e., their apparent diameter in the Stokes−Einstein relation. Taking both effects together, i.e., a somewhat faster diffusion coupled to a larger solubility in region 3, one predicts a permeation rate for nonspherical-shaped penetrants across lipid membranes which is faster than expected from their effective diameter. The accuracy of the experimental data does not allow to justify this conclusion, however.

Permeation Process in the Four-Region Model. On the basis of our simulation results in connection with other available data, we characterize the resistance that is imposed by each of the four membrane regions as follows:

Region 1: Bulk Water. This region behaves essentially as bulk water. Although solubilities and diffusion constants do not remain completely constant across this region, the effect on the total permeation resistance will be close to that of bulk water. That means for most penetrants the resistance is negligible. Only in the case of hydrophobic penetrants (e.g., oxygen or benzene) has the water layer the largest resistance.

Region 2: Interphase. Although this region is the most complicated region considering the variety of atoms found, in its function as resistance to permeation it can be approximated very well by an effective medium with a high dielectric constant and a high viscosity. In this respect it is quite unique and does not resemble any other bulk phase. The high viscosity, a consequence of the high density, results in low diffusion rates in this region. The high dielectric constant resulting from the high mobile charge density allows for a low excess free energy for hydrophilic penetrants. Since the excess free energy profile dominates the permeation resistance, the resistance in region 2 will remain rather low as well. For some penetrants, where the excess free energy in the membrane is close to zero, the diffusion profile may dominate the resistance profile, and the rate-limiting step could be located in region 2. Possible candidates of such molecules are for instance carbon dioxide or certain benzene derivatives which have hydrocarbon/water partition coefficients close to 1.

Region 3: Soft Polymer. This is the most important region considering the permeation process. Since traditional experimental permeation measurements can only be performed for hydrophilic penetrants, the experimentally observed trends are likely to find their origin in this region. Not only because the largest resistances are found in this region, but also because most of the anomalous effects originate from this region. This is essentially due to the high density, which imposes a strong correlation between the chain conformations. In this respect it resembles a soft polymer. As a result, the small penetrants likely diffuse via a hopping mechanism, which possibly accounts for the steep size dependence of the permeation process for the smallest penetrants. The large resistance in this region is due to the low solubility of hydrophilic penetrants in this region, where the charge density is low. In that respect, it behaves not very different from a dense alkane liquid. In another aspect, however, it deviates significantly: the accessible free volume to small penetrants is relatively high, causing an enhanced possibility for the dissolvation of small molecules. Hence, the anomalous size dependency of membrane permeation could also originate from the membrane solubility. Finally, we predict that the anisotropic nature of this region is likely to favor the permeation process of nonspherical molecules above spherical ones.

Region 4: Fluid Decane. Due to the high end group density in this region, it resembles a low-density alkane fluid, like decane. Both the solubility and the diffusion process of this region will therefore be similar to those in decane, a medium characterized by a low dielectric constant and a low viscosity. Because of the low viscosity, the diffusion rate is fast, and therefore the resistance imposed by this region is relatively small compared to region 3, for any kind of penetrant.

Conclusion

Our simulations have shown that the most important function of a lipid membrane, to act as a permeation barrier, is in itself a very complicated one. Due to the inhomogeneous and anisotropic nature of the bilayer, the permeation properties differ considerably for different penetrants. Describing the permeation process with a homogeneous solubility−diffusion model is therefore a definite oversimplification. Within the four-region model, a more appropriate description can be given. We have shown that especially region 3, the dense part of the lipid tails, in general poses the largest resistance to the total permeation process for a wide range of penetrants. This is especially the case with hydrophilic penetrants for which the permeation rates are experimentally accessible. Therefore, this region is also responsible for most of the anomalous effects that are experimentally observed in the permeation process of small penetrants across lipid membranes, compared to the permeation process across bulk alkane phases.

Acknowledgment. This work was supported by the Foundation for Biophysics and the Foundation for National Computer Facilities under the auspices of the Netherlands Organization for Pure Research, NWO. The simulations were performed partly on the Cray-YMP at the Computing Center of Amsterdam and partly on the Cray-YMP at the Computing Center of the Max Planck Society at Garching/Munich, for which the authors are grateful to Fritz Jähnig.

References and Notes

(1) Marrink, S. J.; Berendsen, H. J. C. *J. Phys. Chem.* **1994**, *98*, 4155.
(2) Egberts, E.; Marrink, S. J.; Berendsen, H. J. C. *Eur. Biophys. J.* **1994**, *22*, 423.
(3) Marrink, S. J. Permeation of Small Molecules Across Lipid Membranes−A Molecular Dynamics Study. Thesis, University of Groningen, 1994.
(4) Marrink, S. J.; Sok, R. M.; Berendsen, H. J. C. *J. Chem. Phys.* **1996**, *104*, 9090.
(5) Walter, A.; Gutknecht, J. *J. Membr. Biol.* **1986**, *90*, 207.
(6) Xiang, T.-X.; Anderson, B. D. *J. Membr. Biol.* **1994**, *140*, 111.
(7) Pohorille, A.; Wilson, M. A. *Origins Life Evol. Biosphere* **1995**, *25*, 21.
(8) Guy, R. H.; Honda, D. H. *Int. J. Pharm.* **1984**, *19*, 129.
(9) De Young, L. R.; Dill, K. A. *J. Phys. Chem.* **1990**, *94*, 801.
(10) Lieb, W. R.; Stein, W. D. *Curr. Top. Membr. Transp.* **1971**, *2*, 1.
(11) Sok, R. M. Permeation of Small Molecules Across a Polymer Membrane: a Computer Simulation Study. Thesis, University of Groningen, 1994.
(12) Takeuchi, H. *J. Chem. Phys.* **1990**, *93*, 2062.
(13) Müller-Plathe, F. *J. Chem. Phys.* **1991**, *94*, 3192.
(14) Krishna Pant, P. V.; Boyd, R. H. *Macromolecules* **1993**, *26*, 679.
(15) Bassolino-Klimas, D.; Alper, H. E.; Stouch, T. R. *Biochemistry* **1993**, *32*, 12624.
(16) Bassolina-Klimas, D.; Alper, H. E.; Stouch, T. R. *J. Am. Chem. Soc.* **1995**, *117*, 4118.
(17) Xiang, T.-X.; Anderson, B. D. *Biophys. J.* **1994**, *66*, 561.
(18) Berendsen, H. J. C.; Postma, J. P. M.; van Gunsteren, W. F.; Dinola, A.; Haak, J. R. *J. Chem. Phys.* **1984**, *81*, 3684.
(19) Chiu, S. W.; Clark, M.; Balaji, V.; Subramaniam, S.; Scott, H. L.; Jakobsson, E. *Biophys. J.* **1995**, *69*, 1500.
(20) Tieleman, D. P.; Berendsen, H. J. C. *J. Chem. Phys.*, in press.
(21) Berendsen, H. J. C.; Postma, J. P. M.; van Gunsteren, W. F.; Hermans, J. *Intermolecular Forces*; Pullman, B., Ed.: Reidel: Dordrecht, 1981; pp 331−342.
(22) Fischer, J.; Lago, S. *J. Chem. Phys.* **1983**, *78*, 5750.
(23) Weast, R. C., Ed. *Handbook of Chemistry and Physics*; CRC Press: Boca Raton, FL, 1984.
(24) Battino, R.; Evans, F. D.; Danforth, W. F. *J. Am. Oil Chem. Soc.* **1968**, *45*, 830.
(25) Fishkoff, S.; Vanderkooi, J. M. *J. Gen. Physiol.* **1975**, *65*, 663.
(26) McKinnon, S. J.; Whittenburg, S. L.; Brooks, B. *J. Phys. Chem.* **1992**, *96*, 10497.
(27) Antonenka, Y. N.; Yaguzhinsky, L. S. *Bioelectrochem. Bioenerg.* **1984**, *13*, 85.
(28) De Loof, H.; Harvey, S. C.; Segrest, J. P.; Pastor, R. W. *Biochemistry* **1991**, *30*, 2099.
(29) Müller-Plathe, F.; Rogers. S. C.; van Gunsteren, W. F. *Chem. Phys. Lett.* **1992**, *199*, 237.
(30) Venable, R. M.; Zhang, Y.; Hardy, B. J.; Pastor, R. W. *Science* **1993**, *262*, 223.
(31) Seelig, J.; Ganz, P. *Biochemistry* **1991**, *30*, 9354.
(32) Wimley, W. C.; White, S. H. *Biochemistry* **1993**, *32*, 6307.

JP952956F